Struct Multidisc Optim (2007) 33:351–362
DOI 10.1007/s00158-006-0089-8

RESEARCH PAPER

Optimal design of composite structures for strength and stiffness: an inverse homogenization approach

Robert Lipton · Michael Stuebner

Received: 2 June 2006 / Revised manuscript received: 7 November 2006 / Published online: 20 January 2007

Abstract We introduce a rigorously based numerical method for compliance minimization problems in the presence of pointwise stress constraints. The method is based on new multiscale quantities that measure the amplification of the local stress due to the microstructure. The design method is illustrated for two different kinds of problems. The first identifies suitably graded distributions of fibers inside shaft cross sections that impart sufficient overall stiffness while at the same time adequately control the amplitude of the local stress at each point. The second set of problems are carried out in the context of plane strain. In this study, we recover a novel class of designs made from locally layered media for minimum compliance subject to pointwise stress constraints. The stress-constrained designs place the more compliant material in the neighborhood of stress concentrators associated with abrupt changes in boundary loading and reentrant corners.

Keywords Stress constraints · Optimal structural design

This research is supported by NSF through grant DMS-0406374 and by the Air Force Office of Scientific Research, Air Force Materiel Command USAF, under grant numbers F49620-02-1-0041 and FA9550-05-1-0008.

R. Lipton (✉) · M. Stuebner
Department of Mathematics, Louisiana State University, Baton Rouge, LA 70803, USA
e-mail: lipton@math.lsu.edu

M. Stuebner
e-mail: stuebner@math.lsu.edu

1 Introduction

It is now well established that homogenization theory is an effective tool for the design of composites for optimal structural compliance and natural frequency (see Allaire 2002; Bendsøe and Sigmund 2003; Cherkaev and Kohn 1997; Cherkaev 2000; Lewinski and Telega 2000; Lurie 1993; Olhoff 1996; Tartar 2000). On the other hand, relatively little work has been directed towards the solution of stress-constrained composite design problems. Recently, new efforts have initiated the development of numerical methods for structural optimization in the presence of stress constraints. The investigation given in Duysinx and Bendsøe (1998) provides a numerical method for the stress-constrained minimum volume design problem. The method is carried out using an empirical model known as the Solid Isotropic Microstructure with Penalization (SIMP) model (see Bendsøe and Sigmund 2003). The problem of mean square stress constrained structural optimization for fiber reinforced shafts is taken up in Lipton (2002b). In that work, a numerical algorithm is developed based on a suitable homogenized quantity (the covariance tensor) that rigorously encodes the mean square stress constraints. The work of Allaire et al. (2004) introduces a partial relaxation for topology optimization for minimum mean square stress using finite rank laminates.

The general theory behind the homogenization approach to mean square stress (or gradient) constrained structural optimization is significantly different from the theory of compliance minimization. It is demonstrated in Lipton (2002a) and Lipton (2004b) that the associated relaxed problem formulation requires the use of the derivatives of G-limits in addition to

using the theory of effective properties (G-limits). Alternative theoretical treatments for the related scalar problem of minimizing the mean square distance of the gradient from a target have been developed in the earlier work of Tartar (1994) and subsequent work presented in Velo (2000), Grabovsky (2001), Lipton and Velo (2002), Pedregal (2004), and Donso and Pedregal (2005). These methods can naturally be rephrased in terms of G-limits and their derivatives. All of these methods invoke the use of suitable homogenized or multiscale quantities for the design of local microgeometry. For this reason, these approaches may be considered inverse homogenization methods.

In this paper, we present a new rigorously based numerical approach to the problem of microstructure design for minimum compliance subject to pointwise stress constraints. In this study, the objective is to design a graded microstructure to control local stress in the vicinity of stress concentrations. The methodology used in this study has been developed by the authors in Lipton (2004a), Lipton and Stuebner (2006a), and Lipton and Stuebner (2006b) and is based upon new rigorous multiscale stress criteria that connect the macroscopic or homogenized stress to the local stress at the scale of the microstructure (see Lipton 2003, 2004c). The multiscale criteria are given in terms of quantities dubbed macrostress modulation functions. In this study, we show how to apply these multiscale quantities to develop an inverse homogenization approach for minimum compliance design subject to pointwise stress constraints. The homogenized design formulation considered in this study is expressed in terms of homogenized stress and strain fields and macrostress modulation functions. The homogenized design problem satisfies two requirements: the first is that the homogenized design problem is computationally tractable. The second is that the solution of the homogenized design problem provides the means to identify graded microstructures that deliver the required structural res-ponse while at the same time provide control on the pointwise values of the stress inside the composite.

The design method is illustrated for two different kinds of problems. The first type of problem is to identify suitably graded distributions of fibers inside shaft cross sections that impart sufficient overall stiffness while at the same time adequately control the intensity of the local stress. This problem is solved numerically in Section 3. The second set of examples are carried out in the context of plane strain. In these examples, we consider designs made from locally layered media. In this study, we exhibit novel minimum compliance designs that are subject to pointwise stress constraints (see Section 4). These designs are shown to drastically reduce the pointwise stress below the stress levels seen in the minimum compliance designs. The new stress constrained designs feature zones of compliant material surrounding stress concentrators due to abrupt changes in boundary loading and reentrant corners.

This paper touches on several topics that have been part of the work of Pauli Pedersen. These include material optimization, shape design, and stress constraints. The authors would like to dedicate this article to Professor Pedersen on the occasion of his 70th birthday.

2 Homogenized design formulation and identification of optimally graded fiber reinforced shafts

We start by illustrating our approach for the first design problem. In this study, we consider fiber reinforcement of a long shaft with constant cross section subjected to torsion loading (see Love 1944). The microstructure within the shaft consists of long reinforcement fibers of constant cross section with isotropic shear modulus G_f embedded in a more compliant material with shear modulus G_m. The shaft together with the fibers are right cylinders with generators along the x_3 axis. The cross section of the reinforced shaft is specified by a fixed region Ω in the $x_1 - x_2$ plane. The shaft cross section is divided up into many square cells. Each cell contains a single fiber cross section. The fiber cross section is circular and is centered inside the square cell. The radii of the fiber inside each cell is chosen independently of the others. The characteristic length scale of the square cells relative to the size of the design domain is denoted by ε. Our design problem is carried out when the total fiber cross-sectional area is constrained to be 40% and for $\varepsilon = 0.1$. The goal of the design problem is to identify a graded distribution of fibers across the cross section such that the following requirements are met:

I. The reinforced shaft has a torsional rigidity that is acceptable.
II. The magnitude of the local pointwise stress inside the composite is controlled over a designated subset of the cross section.

To illustrate the ideas, we develop the inverse homogenization design method within the context of this problem. The inverse homogenization design method is a top–down design approach. First, a well-posed homogenized design problem is developed. This design problem is given in terms of design variables that reflect the local microgeometry inside the composite. For the problem treated in this study, the design variable for the homogenized design problem is given by the

local density of fibers $\theta_f(\mathbf{x})$. The homogenized design problem is then solved to obtain an optimal density function $\hat{\theta}_f(\mathbf{x})$. With the optimal density in hand, we use it to recover an explicit-graded fiber design that has structural properties close to that of the optimal homogenized design and satisfies prescribed pointwise stress constraints. Such a fiber design is shown in Fig. 5. The subsections are organized as follows, we begin by describing the homogenized design problem and then provide the explicit link between homogenized designs and graded fiber reinforced designs that satisfy pointwise stress constraints.

2.1 Homogenized design problem

The design variable for the homogenized design problem is given by the density function $\theta_f(\mathbf{x})$. This function is interpreted as providing the local area fraction of the fiber phase in a homogenized design. The resource constraint on the fiber phase is given by

$$\int_\Omega \theta_f(\mathbf{x})\, dx_1 dx_2 \leq \Theta \times (Area\ of\ \Omega), \tag{2.1}$$

where $0 < \Theta < 1$. At each point, the local area fraction satisfies the box constraint given by

$$0 < \theta_f^{\min} \leq \theta_f \leq \theta_f^{\max} < 1. \tag{2.2}$$

Here, the upper and lower bounds given in (2.2) correspond to the entire design domain being filled with composite material. In this treatment, the local fiber area fraction θ_f changes continuously with position according to the condition

$$|\theta_f(\mathbf{x}) - \theta_f(\mathbf{x}+\mathbf{h})| \leq K|\mathbf{h}|. \tag{2.3}$$

Here, the constant K is prescribed by the designer. The universe of admissible designs given by all local area fractions θ_f satisfying the resource constraint, box constraints, and (2.3) is denoted by D_Θ.

The compliance in shear for the matrix and fiber are given by $S_m = (2G_m)^{-1}$ and $S_f = (2G_f)^{-1}$, respectively. Here, the matrix is more compliant and $S_m > S_f$. For a given $\theta_f(\mathbf{x})$, we introduce the effective shear compliance $S^E(\theta_f(\mathbf{x}))$ associated with a locally periodic microgeometry made from fibers with circular cross sections centered inside square unit cells. The unit period cell for this configuration is denoted by Q. The area fraction of Q occupied by the fiber cross section is set to $\theta_f(\mathbf{x})$. The shear compliance inside Q is written $S(\theta_f(\mathbf{x}), \mathbf{y})$ and takes the value S_f for points $\mathbf{y}$ in the fiber and S_m for $\mathbf{y}$ in the matrix. The unit vectors $\mathbf{e}^1 = (1, 0)$ and $\mathbf{e}^2 = (0, 1)$ are introduced and for each $\mathbf{x}$ in Ω, we introduce the periodic fluctuating stress potentials $w^i(\mathbf{x}, \mathbf{y})$, $i = 1, 2$ that solve the microscopic equilibrium equation

$$-\mathrm{div}_{\mathbf{y}}\left(S(\theta_f(\mathbf{x}), \mathbf{y})(\nabla_{\mathbf{y}} w^i(\mathbf{x}, \mathbf{y}) + \mathbf{e}^i)\right) = 0 \tag{2.4}$$

for $\mathbf{y}$ in Q. Here, the $\mathbf{x}$ coordinate appears a parameter and all differentiations are carried out with respect to the $\mathbf{y}$ variable. The effective compliance tensor is a function of the local area fraction of fibers θ_f and from symmetry the effective compliance tensor is isotropic and given by

$$\left[S^E(\theta_f(\mathbf{x}))\right]_{ij} = s^E(\theta_f(\mathbf{x}))\delta_{ij} \tag{2.5}$$

where the effective compliance is given by

$$s^E(\theta_f(\mathbf{x})) = \left(\int_Q S(\theta_f(\mathbf{x}), \mathbf{y})\left(\partial_{y_1} w^1(\mathbf{x}, \mathbf{y}) + \mathbf{e}_1^1\right) d\mathbf{y}\right). \tag{2.6}$$

A graph of s^E plotted as a function of θ_f is given in Fig. 1 for the choice $S_m = 0.5$ and $S_f = 0.25$.

The macroscopic stress potential ϕ^H vanishes on the boundary of the shaft cross section and satisfies

$$-\mathrm{div}\left(S^E(\theta_f)\nabla\phi^H\right) = 1 \tag{2.7}$$

inside the cross section. The torsional rigidity for the homogenized shaft cross section made from a homogenized material with compliance $S^E(\theta_f)$ is given by

$$\mathcal{R}(\theta_f) = 2\int_\Omega \phi^H\, dx_1 dx_2. \tag{2.8}$$

The macroscopic stress in the homogenized shaft is given by $\sigma^H = R\nabla\phi^H$ where R is the rotation matrix associated with a counterclockwise rotation of $\pi/2$ radians.

The multiscale stress criterion is given in terms of the macrostress modulation function introduced in Lipton

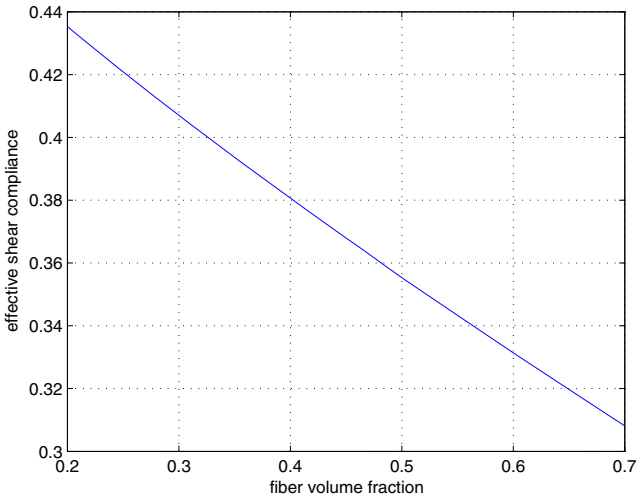

Fig. 1 Plot of s^E

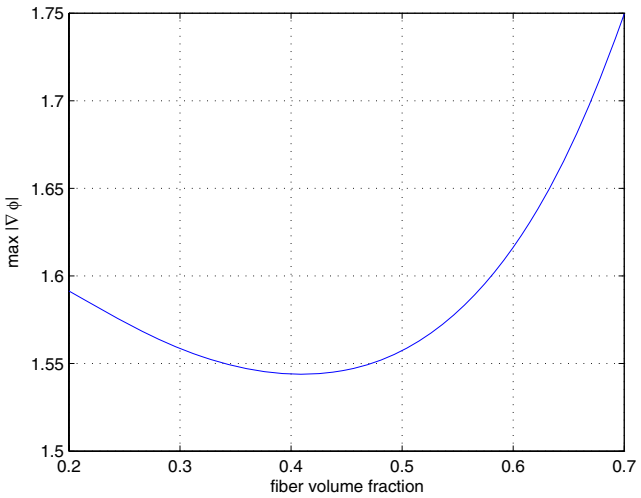

Fig. 2 Plot of $A(\theta_f)$

(2003). The macrostress modulation function captures the interaction between the macroscopic stress $\sigma^H(\mathbf{x})$ and the microstructure. The microscopic response to the imposed macroscopic stress is given by

$$\sigma(\mathbf{x},\mathbf{y}) = R\left[\sum_{i=1}^{2}(\nabla_{\mathbf{y}}(w^i(\mathbf{x},\mathbf{y})) + \mathbf{e}^i)\partial_{x_i}\phi^H(\mathbf{x})\right].$$

The relevant interaction is described by the macrostress modulation function $f(\theta_f, \sigma^H)$ given by

$$f\left(\theta_f(\mathbf{x}), \sigma^H(\mathbf{x})\right) = \sup_{\mathbf{y}\ \text{in}\ Q}\left\{|\sigma(\mathbf{x},\mathbf{y})|\right\}. \tag{2.9}$$

Physically, the macrostress modulation provides an upper envelope on the oscillating pointwise local stress in the composite (see Lipton 2003).

From the symmetry of the microstructure, it easily follows that macrostress modulation for a locally periodic microgeometry made from fibers with circular cross sections centered inside square unit cells is of the form

$$f\left(\theta_f(\mathbf{x}), \sigma^H(\mathbf{x})\right) = A(\theta_f(\mathbf{x}))\left|\nabla\phi^H(\mathbf{x})\right|, \tag{2.10}$$

where for $0 < \theta_f^{\min} \le \theta_f \le \theta_f^{\max} < 1$,

$$A(\theta_f) = \sup_{\mathbf{y}\ \text{in}\ Q}\left\{|\nabla_{\mathbf{y}} w^1(\mathbf{x},\mathbf{y}) + \mathbf{e}^1|\right\}. \tag{2.11}$$

A graph of the local stress amplification factor $A(\theta_f)$ as function of θ_f is given in Fig. 2 for the choice $S_m = 0.5$ and $S_f = 0.25$.

We enforce the stress constraint by adding a penalty term to the torsional rigidity and the homogenized design problem is to minimize

$$L(\theta_f) = -\mathcal{R}(\theta_f) + l\int_\Omega \left(f(\theta_f, \nabla\phi^H)\right)^p\, dx_1 dx_2, \tag{2.12}$$

over all θ_f in D_Θ where $l > 0$ and ϕ^H satisfies

$$-\text{div}\left(S^E(\theta_f)\nabla\phi^H\right) = 1 \tag{2.13}$$

and vanishes at the boundary. The computational examples are carried out for a domain with reentrant corners of interior angle $3\pi/2$. In view of the strength of the associated singularity at the reentrant corners the power "p" appearing in the penalty term is chosen to be less than 3. We mention in closing that (2.3) provides a constraint on the spatial variation of the homogenized designs. This constraint provides the compactness necessary for a well-posed design problem (Lipton 2004a). We point out that in our numerical simulations for the fiber reinforced shaft, we have relaxed the constraint (2.3) and discretized θ_f using linear triangular elements.

2.2 Identification of graded fiber design from the homogenized design

In this subsection, it is shown how to use the optimal design $\hat{\theta}_f$ for the homogenized problem to identify a graded fiber design satisfying the requirements (I) and (II). The examples considered in this treatment are given for a structural domain specified by an "X"-shaped cross section. All interior angles for the reentrant corners are fixed at $3\pi/2$ radians. The tip-to-tip length of each leg of the "X"-shaped domain is 2 cm. The width of each leg is 2/3 cm. To describe the graded fiber composite, the shaft cross section Ω is partitioned into the N square subdomains $\mathcal{S}^k$, $k = 1, \ldots, N$ and $\Omega = \cup_k^N \mathcal{S}^k$. The side length of these subdomains is given by ε.

The building block for the microstructure is the square unit cell filled with a centered circular fiber cross section. The area fraction of the fiber phase inside the unit cell is given by θ_f. A microstructure is obtained by rescaling the unit cell by the factor $\varepsilon \times \nu$ so that it becomes the period cell for a $\varepsilon \times \nu$ periodic composite. A graded fiber composite is constructed by placing a $\varepsilon \times \nu$ periodic composite inside each square subdomain $\mathcal{S}^k$. The area fraction of fibers in each subdomain is given by the constant θ_f^k and these constants can change between subdomains. We note that choosing $\nu = 1$ corresponds to placing one fiber cross section inside $\mathcal{S}^k$. Higher values of ν correspond to progressively finer periodic distributions of fiber cross sections inside $\mathcal{S}^k$.

For future reference, this type of locally periodic microstructure will be called a (ε, ν)-graded periodic fiber microstructure.

The local piecewise constant shear compliance for the (ε, ν)-graded periodic fiber microstructure is denoted by $S^{\varepsilon,\nu}$. The stress potential for this microstructure is denoted by $\phi^{\varepsilon,\nu}$ and vanishes on the boundary of the cross section. The stress potential satisfies the equilibrium equation

$$-\text{div}\ (S^{\varepsilon,\nu}\nabla\phi^{\varepsilon,\nu}) = 1. \tag{2.14}$$

The torsional rigidity of the cross section is given by

$$\mathcal{R}^{\varepsilon,\nu} = 2\int_{\Omega} \phi^{\varepsilon,\nu}\, dx_1 dx_2. \tag{2.15}$$

The nonzero components of the inplane stress are denoted by the vector $\sigma^{\varepsilon,\nu} = (\sigma^{\varepsilon,\nu}_{13}, \sigma^{\varepsilon,\nu}_{23})$ and are related to the gradient of the stress potential according to

$$\sigma^{\varepsilon,\nu} = R\nabla\phi^{\varepsilon,\nu}. \tag{2.16}$$

Here, R is the matrix corresponding to a counterclockwise rotation of $\pi/2$ and $|\sigma^{\varepsilon,\nu}| = |\nabla\phi^{\varepsilon,\nu}|$.

The relation between the optimal design for the homogenized problem and the pointwise stress and torsional rigidity for the (ε, ν)-graded periodic fiber microstructure is given in the following Theorem (see Lipton 2004a; Lipton and Stuebner 2006b).

Theorem 2.1 *Identification of graded microstructure. Given the minimizing density $\hat{\theta}_f$ and associated stress potential $\hat{\phi}^H$ for the homogenized problem, we consider sets of the form*

$$A_T = \left\{\mathbf{x}\in\Omega:\ f\left(\hat{\theta}_f(\mathbf{x}), \nabla\hat{\phi}^H(\mathbf{x})\right) \le T\right\}. \tag{2.17}$$

For fixed choices of $\delta > 0$ and $t > T$, one can choose ε and ν small enough such that the (ε, ν)-graded periodic microstructure for which the the part of A_T over which the stress constraint

$$|\nabla\phi^{\varepsilon,\nu}(\mathbf{x})| \le t \tag{2.18}$$

is violated has measure (area) less than δ and

$$|\mathcal{R}^{\varepsilon,\nu} - \mathcal{R}(\hat{\theta}_f)| < \delta, \tag{2.19}$$

with

$$\sum_{k=1}^{\hat{N}} |\mathcal{S}^k|\hat{\theta}^k_f \le \Theta \times (\mathit{Area\ of}\ \Omega) + \delta. \tag{2.20}$$

For these designs, the area fractions of the fibers inside each $\mathcal{S}^k$ are denoted by $\hat{\theta}^k_f$ and are chosen according to

$$\hat{\theta}^k_f = \frac{1}{|\mathcal{S}^k|} \times \int_{\mathcal{S}^k} \hat{\theta}_f(\mathbf{x}) dx_1 dx_2. \tag{2.21}$$

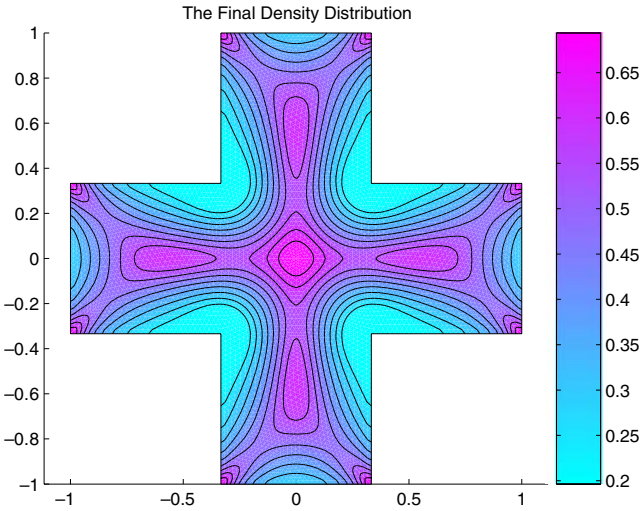

Fig. 3 Grey scale plot of the local area fraction of fibers $\hat{\theta}_f(\mathbf{x})$

The homogenized design formulation together with the identification Theorem comprise the inverse homogenization method for identifying microstructures that satisfy pointwise stress constraints while delivering a torsional rigidity close to that given by the optimal design $\hat{\theta}_f$ for the homogenized design problem.

3 Inverse homogenization and graded fiber designs for the X-shaped cross section

In this section, we demonstrate the methodology for fiber reinforced shafts. The calculations were carried out using the gradient minimization algorithm introduced in Lipton and Stuebner (2006b) and Lipton and Stuebner (2006a). All calculations are done for the

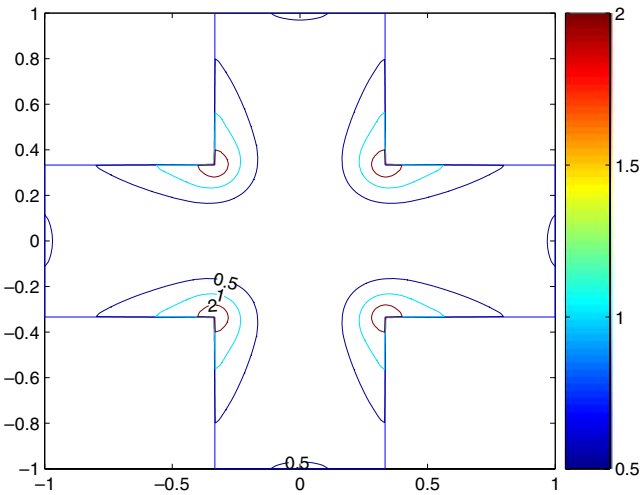

Fig. 4 Contour plot of $f(\hat{\theta}_f(\mathbf{x}), \nabla\phi^H(\mathbf{x}))$

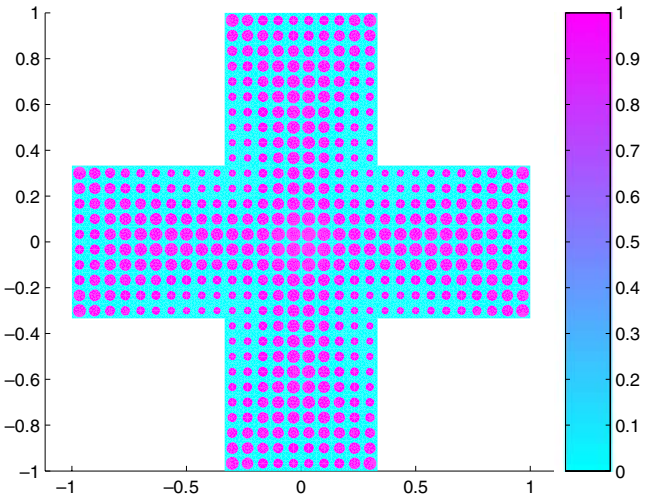

Fig. 5 Graded fiber design

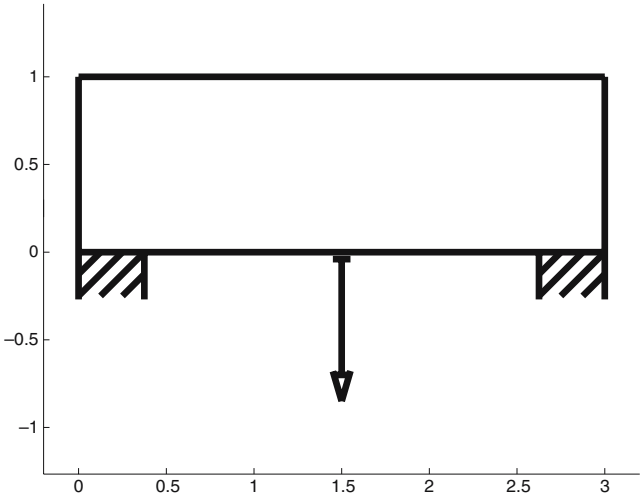

Fig. 7 Loading for the rectangular domain for the plane strain problem

choice $p = 1$ in the Lagrangian (2.12). The shear stiffness of the matrix is assigned the value $G_m = 1\,GPa$ and the shear stiffness of the fiber phase is assigned the value $G_f = 2\,GPa$. For these choices, $S_m = 1/(2G_m) = 0.5$ and $S_f = 1/(2G_f) = 0.25$. For this example, θ_f is constrained to lie between $0.2 \leq \theta_f \leq 0.7$ and $\int_\Omega \theta_f = 0.4 \times Area\,of\,\Omega$. A plot of the fiber density field $\hat{\theta}_f$ is given in Fig. 3. The contour plots of the macrostress modulation function $f(\hat{\theta}_f(\mathbf{x}), \nabla\hat{\phi}^H(\mathbf{x}))$ is given in Fig. 4.

The (ε, ν)-graded periodic microstructure is constructed from the optimal homogenized design according to the prescription of Theorem 2.1. Here, we compute the average of $\hat{\theta}_f(\mathbf{x})$ over each square $\mathcal{S}^k$ according to (2.21) and denote it by $\hat{\theta}_f^k$. The area fraction of the fibers in $\mathcal{S}^k$ is set to $\hat{\theta}_f^k$. The design is computed for the choice $\varepsilon = 0.1$ and $\nu = 1$. The discrete fiber design is displayed in Fig. 5.

The level lines of the magnitude of the stress field in the actual fiber reinforced design is plotted in Fig. 6. It follows from Figs. 4 and 6 that the pointwise stress behavior is well represented by the level curves of the macrostress modulation function for the optimal homogenized design.

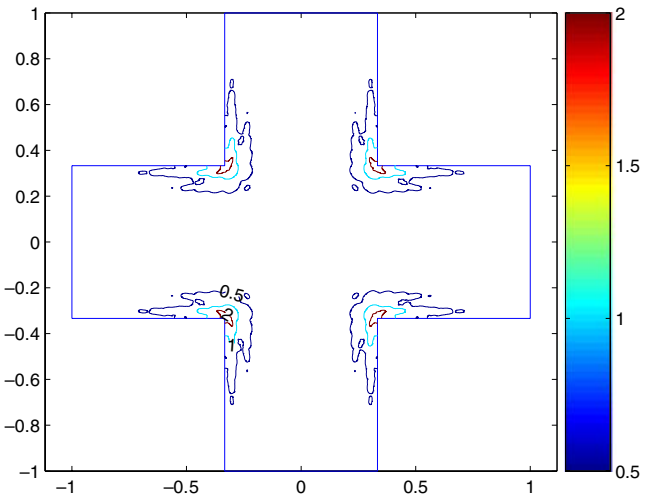

Fig. 6 Contour plot of the magnitude of the local stress amplitude

4 Graded locally layered media and two dimensional elastic design

For our second set of examples, we consider a long beam of fixed cross section and we suppose that the loading is the same for every cross section. This is the classic case of plain strain loading (Love 1944). We first consider rectangular cross sections with loading and boundary conditions illustrated in Fig. 7. For this case, the microgeometry is made up of locally layered material made from two linearly elastic components. The layers consist of long rectangular fibers with constant cross section with generators parallel to the beam. The design variables are the relative thicknesses of the layers and their orientation and these can change across the rectangular cross section as indicated in Fig. 8.

In this section, we generate optimal locally layered designs for three distinct design criteria. The first is

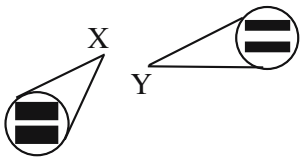

Fig. 8 The local layer thickness and oreintation can change across the cross section

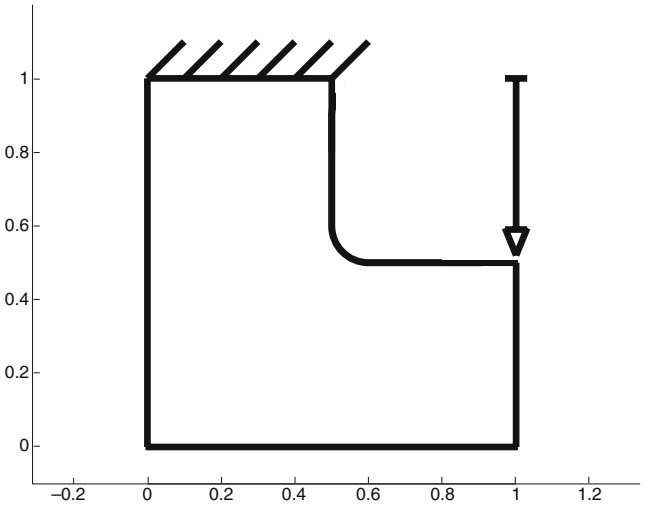

Fig. 9 Loading for the L-shaped domain for the plane strain problem

to design for minimum overall compliance, the second is to design for pointwise stress minimization and the third is to design for minimum compliance subject to a penalty on the magnitude of the pointwise stresses. The homogenization methodology for optimal compliance design requires one to use only the effective elastic properties of the layered elastic medium (see Bendsøe and Sigmund 2003). However, to design for the second two criteria, we will need to also use the macrostress modulation function associated with layered materials.

The two component materials are elastically isotropic and well ordered with Young's moduli $E_1 > E_2$ and equal Poisson's ratio $\nu_1 = \nu_2$. The effective elastic tensor for the layered material depends upon the relative local relative layer thickness of material one and the layer orientation. The local layer thickness of material one is denoted by θ_1. The layer orientation is specified by the local unit vector normal to the layers and is denoted by $\mathbf{n}$. The elastic tensor for each material is denoted by A_1 and A_2 and the formula for the effective elasticity is given by Francfort and Murat (1987)

$$A^L(\theta_1, \mathbf{n}) = A_1 + \theta_1 \left[(A_1 - A_2)^{-1} + (1-\theta_1)\Gamma(\mathbf{n})\right]^{-1}, \quad (4.1)$$

where $\Gamma(\mathbf{n})$ is given by

$$\Gamma(\mathbf{n})\eta : \eta = \frac{1}{\mu_1}\left(|\eta\mathbf{n}|^2 - (\eta\mathbf{n}\cdot\mathbf{n})^2\right) + \frac{1}{2\mu_1+\lambda_1}(\eta\mathbf{n}\cdot\mathbf{n})^2, \quad (4.2)$$

for any constant strain η. Here, the shear modulus μ_1 and Lame coefficient λ_1 are those associated with plane strain.The homogenized stress σ^H is related to the homogenized strain e^H by

$$\sigma^H = A^L(\theta_1, \mathbf{n})e^H. \quad (4.3)$$

The elastic strain $e^H = 1/2(u^H_{i,j} + u^H_{j,i})$ is the symmetrized gradient of the elastic displacement $\mathbf{u}^H$. The elastic displacement is the solution of the equilibrium problem

$$\text{div}\left(A^L e^H\right) = 0, \quad (4.4)$$

and satisfies the displacement and traction conditions given in Fig. 7. Following Stuebner (2006) the macro stress modulation function associated with material one for the layered material is given by

$$f_1\left(\theta_1, \sigma^H(\mathbf{x})\right) = |A_1\overline{\zeta}|^2, \quad (4.5)$$

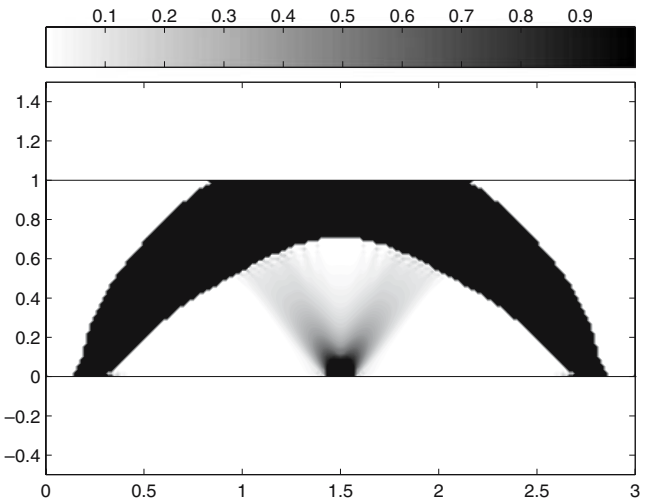

Fig. 10 Grey scale plot of $\hat{\theta}_1(\mathbf{x})$ for the minimum compliance design

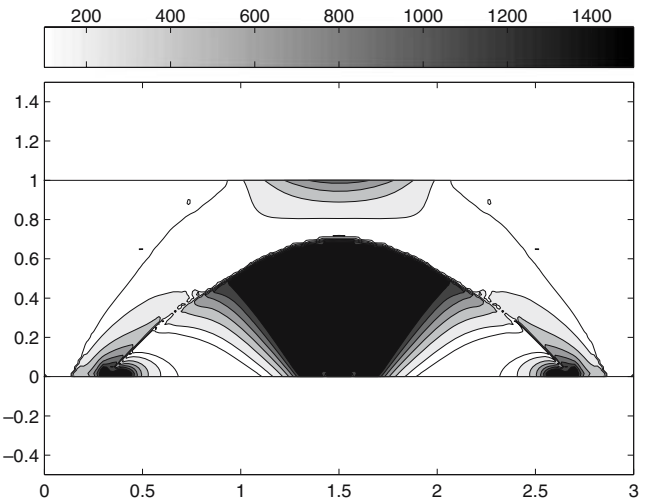

Fig. 11 Contour plot of $f_1(\hat{\theta}_1(\mathbf{x}), \sigma^H(\mathbf{x}))$ for the minimum compliance design

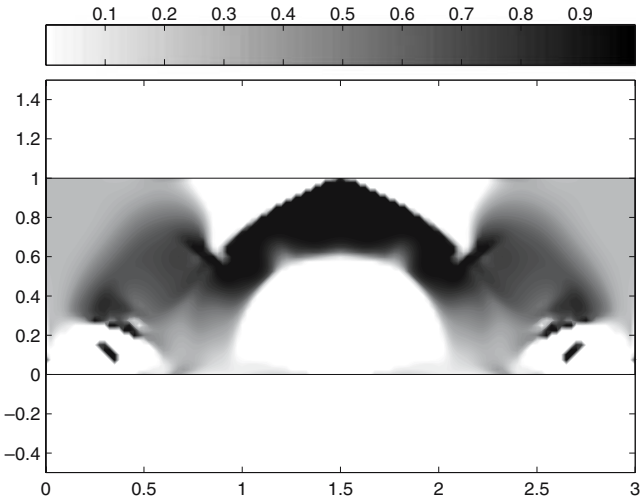

Fig. 12 Grey scale plot of $\hat{\theta}_1(\mathbf{x})$ for the minimum stress design

where

$$\overline{\zeta} = A_1\overline{\eta} + \frac{(1-\theta_1)}{2}A_1(\mathbf{p}\otimes\mathbf{n} + \mathbf{n}\otimes\mathbf{p}) \tag{4.6}$$

and $\overline{\eta} = (A^L)^{-1}\sigma^H$. Here, $\otimes$ denotes the tensor product of two vectors and

$$\mathbf{p} = \frac{\Delta\mu}{\langle\tilde{\mu}\rangle}(2\overline{\eta}\mathbf{n} - tr\{\overline{\eta}\}\mathbf{n}) + \frac{\Delta\kappa}{\langle\tilde{\mu}\rangle}tr\{\overline{\eta}\}\mathbf{n} - \\ -\frac{\langle\tilde{\kappa}\rangle}{\langle\tilde{\mu}\rangle}\left(\frac{\Delta\mu(2\overline{\eta}\mathbf{n}\cdot\mathbf{n} - tr\{\overline{\eta}\}) + \Delta\kappa tr\{\overline{\eta}\}}{\langle\tilde{\mu}\rangle + \langle\tilde{\kappa}\rangle}\right)\mathbf{n}, \tag{4.7}$$

where $\Delta\mu = \mu_2 - \mu_1$, $\Delta\kappa = \kappa_2 - \kappa_1$, $\langle\tilde{\mu}\rangle = (1-\theta_1)\mu_1 + \theta_1\mu_2$, and $\langle\tilde{\kappa}\rangle = (1-\theta_1)\kappa_1 + \theta_1\kappa_2$.

The explicit link relating the local stress in a locally layered composite to the macro stress modulation is analogous to Theorem 2.1 and is derived in Lipton and Stuebner (2006b). The physical significance of the macrostress modulation function is that it provides an upper envelope on the local pointwise stress amplitude inside material one when the layered microstructure is sufficiently fine (see Lipton and Stuebner 2006b).

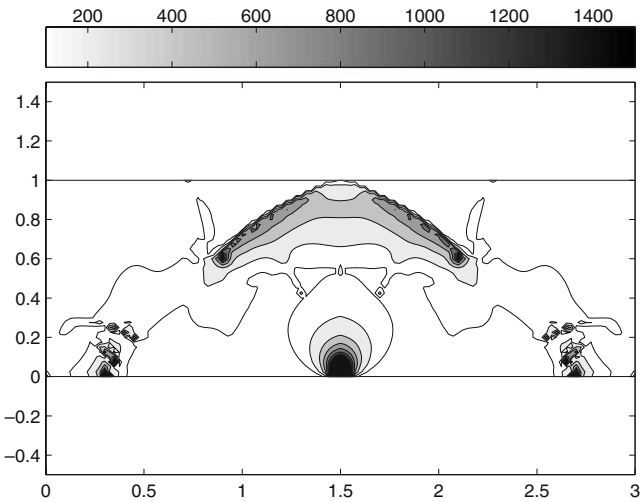

Fig. 13 Contour plot of $f_1(\hat{\theta}_1(\mathbf{x}), \sigma^H(\mathbf{x}))$ for the minimum stress design

The design variables for this problem are the local area fraction $\theta_1(\mathbf{x})$ of material one used in the layers and the layer orientation $\mathbf{n}(\mathbf{x})$. Here, the layer orientation is written

$$\mathbf{n}(\mathbf{x}) = (\sin\gamma(\mathbf{x}), \cos\gamma(\mathbf{x}))$$

where $\gamma(\mathbf{x})$ is the local layer angle. As before, $\theta_1(\mathbf{x})$ is free to change inside the design domain subject to the constraints given by (2.1), (2.2), and (2.3). Here, the box constraints are given by $0 \le \gamma < \pi$, $0.01 \le \theta_1 \le 0.99$, $\int_\Omega \theta_1 = 0.4 \times Area\,of\,\Omega$, $E_1 = 300Gpa$, $E_2 = 30Gpa$, and $\nu_1 = \nu_2 = 1/3$. We reiterate that the box constraints on θ_1 ensure that the design domain is completely filled with composite material.

The overall compliance of the structure is given by

$$C(\theta_1, \gamma) = \int \mathbf{g}\cdot\mathbf{u}^H\, ds, \tag{4.8}$$

where the integral is taken over the boundary of the design domain and $\mathbf{g}$ is the boundary traction field. The design problem for minimizing the overall compliance is given by

$$\min_{\theta_1\,\gamma}\{C(\theta_1,\gamma)\},$$
$$\text{subject to constraints on } \theta_1. \tag{4.9}$$

This design problem is shown to be well posed in Lipton and Stuebner (2006b). The optimal area fraction distribution for this problem is denoted by $\hat{\theta}_1$ and is displayed in Fig. 10. The level curves of the associated macrostress modulation function for material one are plotted in Fig. 11.

For the second design problem, we minimize the macrostress modulation function associated with the stiff material (material one) over the cross section. Here, the function to be optimized is given by

$$M(\theta_1, \gamma) = \int (f_1(\theta_1, \sigma^H))^p\, d\mathbf{x}, \tag{4.10}$$

Table 1 Technical data for the arch

Optimized for:	phase 1	$C(\theta_1,\gamma)$	$M(\theta_1,\gamma)$
Compliance	40.461%	1.876	1563.462
Stress	40.122%	5.777	557.467
Compliance and stress	40.364%	3.428	587.924

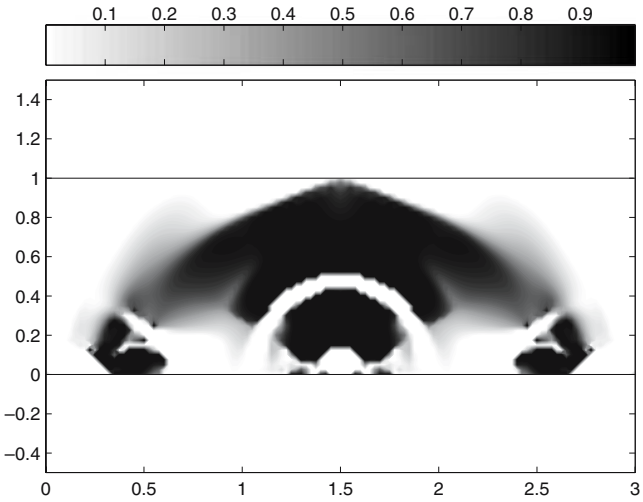

Fig. 14 Grey scale plot of $\hat{\theta}_1(\mathbf{x})$ for the stress penalized minimum compliance design

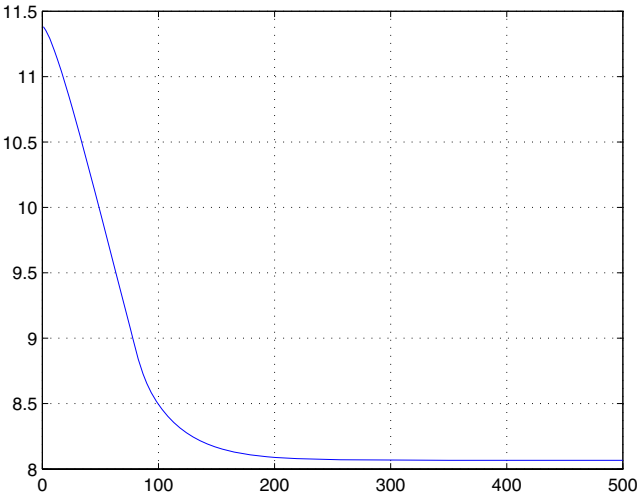

Fig. 16 Convergence history for $C(\theta_1, \gamma)$ for minimum compliance design

where the integral is taken over the design domain and $1 \leq p < \infty$. The design problem for minimizing the local stress inside material one is given by

$$\min_{\theta_1 \gamma} \{M(\theta_1, \gamma)\},$$

$$\text{subject to constraints on } \theta_1. \tag{4.11}$$

This design problem is shown to be well posed in Lipton and Stuebner (2006b). For this example, we choose $p = 1$.

The optimal area fraction distribution for this problem is denoted by $\hat{\theta}_1$ and is displayed in Fig. 12. The level curves of the associated macrostress modulation function are plotted in Fig. 13. The comparison of Figs. 11 and 13 shows that the zones of high stress amplitude are dramatically reduced by the minimum stress design displayed in Fig. 12. While the overall compliance for the minimum stress design is three times higher than the minimum compliance design (see Table 1).

Last, the compliance minimization subject to a penalty on the pointwise stress inside material one is given by

$$\min_{\theta_1 \gamma} \{C(\theta_1, \gamma) + \ell \times M(\theta_1, \gamma)\},$$

$$\text{subject to constraints on } \theta_1. \tag{4.12}$$

where ℓ is the Lagrange multiplier for the stress constraint.

The optimal area fraction distribution for this problem is denoted by $\hat{\theta}_1$ and is displayed in Fig. 14. The level curves of the associated macrostress modulation

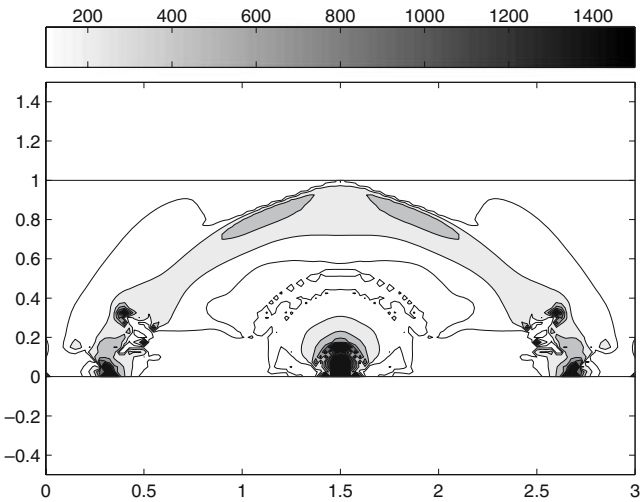

Fig. 15 Contour plot of $f_1(\hat{\theta}_1(\mathbf{x}), \sigma^H(\mathbf{x}))$ for the stress penalized minimum compliance design

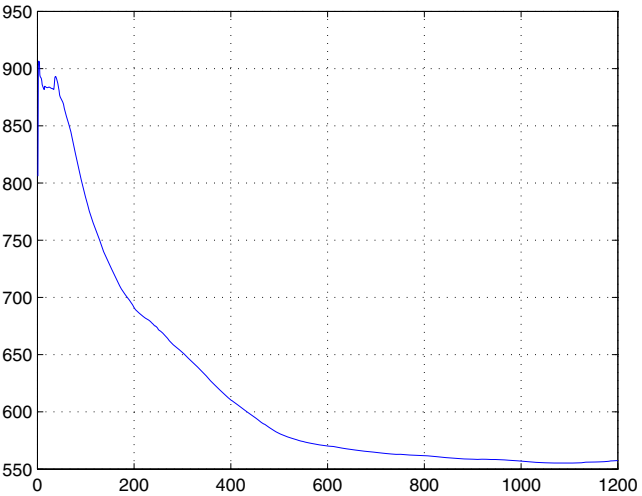

Fig. 17 Convergence history for $M(\theta_1, \gamma)$ for minimum stress design

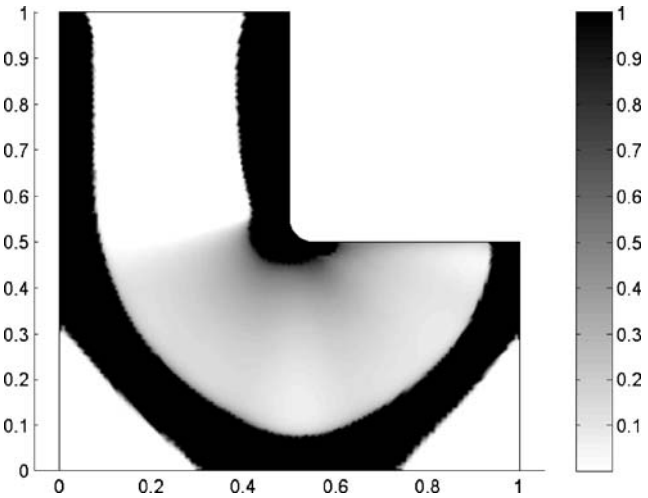

Fig. 18 Grey scale plot of $\hat{\theta}_1(\mathbf{x})$ for the minimum compliance design for the L-shaped domain

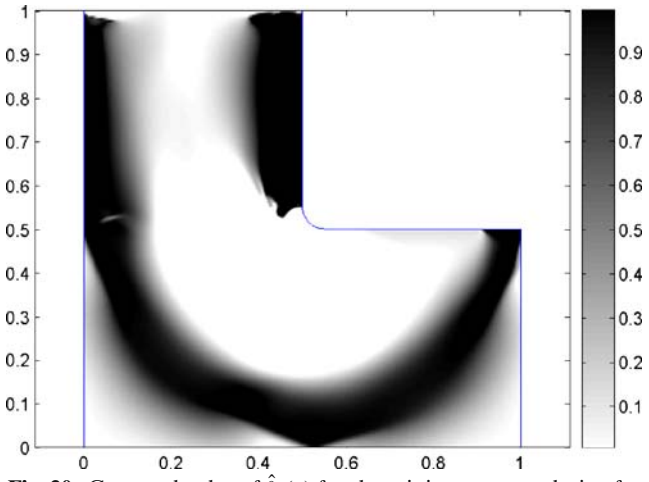

Fig. 20 Grey scale plot of $\hat{\theta}_1(\mathbf{x})$ for the minimum stress design for the L-shaped domain

function are plotted in Fig. 15. The comparison of Figs. 11 and 15 shows that the zones of high stress amplitude seen in the design for compliance minimization are dramatically reduced inside the design obtained from the stress penalized compliance minimization Fig. 14. Table 1 shows that the overall compliance for the stress penalized design is twice as high as the compliance minimized design. It is interesting to note that the stress penalized design surrounds the regions of high stress amplitude with compliant material. This diminishes the effect of the stress concentrations arising from the abrupt change in boundary loading.

In each of these examples, we relaxed the constraint (2.3) and all of the optimizations were carried out using square elements with bilinear shape functions for both the elastic field variables and θ_1. The runs were carried out for a FEM mesh consisting of roughly 11,000 elements. The convergence histories for the minimum compliance design and minimum stress design are given in Figs. 16 and 17.

The final two examples are carried out for the L-shaped design domain. This domain, together with the boundary conditions and loading, is shown in Fig. 9. Here, we compare the solutions to the minimum compliance design problem (4.9) with the minimum local stress design problem (4.11) posed on the L-shaped cross section. As seen in Fig. 9, the L-shaped domain has a rounded reentrant corner that provides a stress concentration.

The design problems are carried out subject to the constraint that 40% of the cross-sectional area is oc-

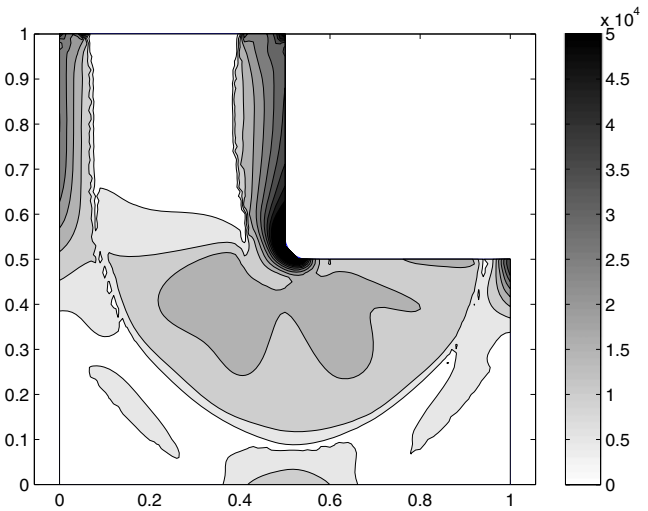

Fig. 19 Contour plot of $f_1(\hat{\theta}_1(\mathbf{x}), \sigma^H(\mathbf{x}))$ for the minimum compliance design for the L-shaped domain

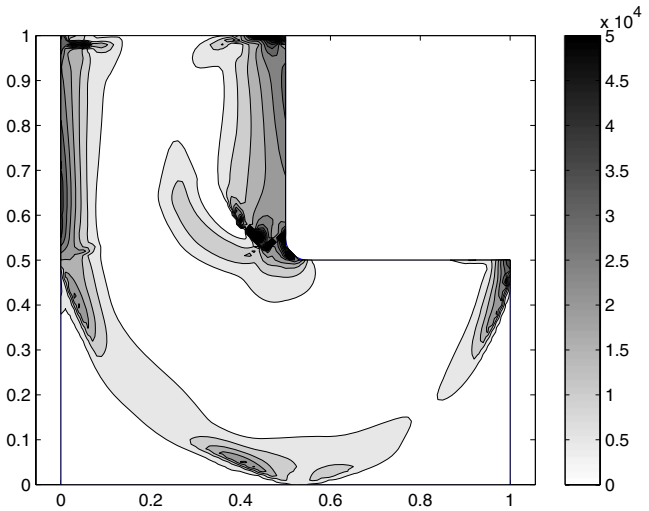

Fig. 21 Contour plot of $f_1(\hat{\theta}_1(\mathbf{x}), \sigma^H(\mathbf{x}))$ for the minimum stress design for the L-shaped domain

Table 2 Technical data for the L-shaped domain

Optimized for:	phase 1	$C(\theta_1, \gamma)$	$M(\theta_1, \gamma)$
Compliance	40.062%	6.525	7197.569
Stress	39.793%	11.986	4737.866

cupied by material one. The optimal distribution of area fraction of material one $\hat{\theta}_1$ for the minimum compliance design problem (4.9) is displayed in Fig. 18. The associated level curves of the macrostress modulation function for material one are plotted in Fig. 19. The optimal distribution of area fraction of material one $\hat{\theta}_1$ for the minimum pointwise stress design problem (4.11) is displayed in Fig. 20 and the associated level curves of the macrostress modulation function for material one are plotted in Fig. 21. Table 2 shows that the minimum compliance design has half the compliance as that of the minimum stress design. On the other hand comparison of Figs. 19 and 21 show that the upper envelope for the pointwise stress intensity as given by the level lines of the macrostress modulation function is significantly lower for the minimum stress design problem. Comparison of Figs. 18 and 20 show that the minimum stress design problem removes the highest concentration of stiff material away from the reentrant corner. In these two examples, we have relaxed the constraint (2.3) and all of the optimizations were carried out using triangular elements with linear shape functions for both the elastic field variables and θ_1. The runs were carried out for a FEM mesh consisting of roughly 72,000 elements. The convergence histories for the objective function for the minimum stress design is given in Fig. 22.

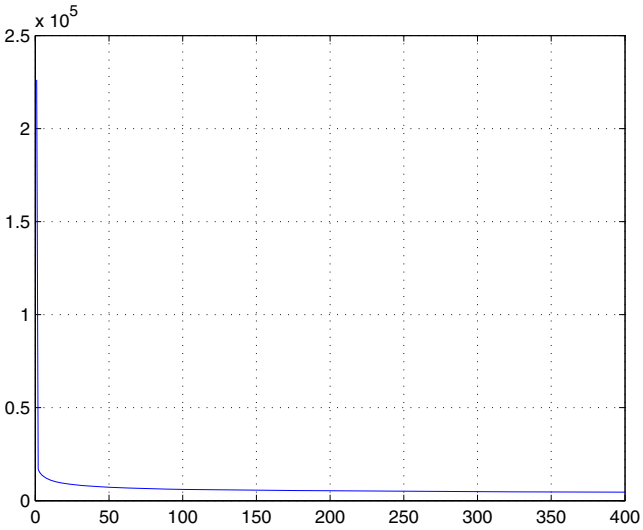

Fig. 22 The convergence history for $M(\theta_1, \gamma)$ for minimum stress design for the L-shaped domain

References

Allaire G (2002) Shape optimization by the homogenization method. Springer, Berlin Heidelberg New York

Allaire G, Jouve F, Mallot H (2004) Topology optimization for minimum stress design with the homogenization method. Struct Multidisc Optim 28:87–98

Bendsøe MP, Sigmund O (2003) Topology optimization, theory, methods and applications. Springer, Berlin Heidelberg New York

Cherkaev A, Kohn RV (1997) Topics in the mathematical modelling of composite materials. Progress in nonlinear differential equations and their applications. Birkhäuser, Boston

Cherkaev A (2000) Variational methods for structural optimization. Springer, Berlin Heidelberg New York

Donoso A, Pedregal P (2005) Optimal design of 2D conducting graded materials by minimizing quadratic functionals in the field. Struct Multidisc Optim 30:360–367

Duysinx P, Bendsøe MP (1998) Topology optimization of continuum structures with local stress constraints. Int J Numer Methods Eng 43:1453–1478

Francfort G, Murat F (1987) Homogenization and optimal bounds in linear elasticity. Arch Ration Mech Anal 94: 307–334

Grabovsky Y (2001) Optimal design problems for two-phase conducting composites with weakly discontinuous objective functionals. Adv Appl Math 27:683–704

Kohn RV, Strang G (1986) Optimal design and relaxation of variational problems. Commun Pure Appl Math 34(1): 113–137, (2):139–182, (3):357–377

Lewinski T, Telega JJ (2000) Plates, laminates and shells. Asymptotic analysis and homogenization. World Scientific, Singapore

Lipton R (2002a) Relaxation through homogenization for optimal design problems with gradient constraints. J Optim Theory Appl 114:27–53

Lipton R (2002b) Design of functionally graded composite structures in the presence of stress constraints. Int J Solids Struct 39:2575–2586

Lipton R (2003) Assessment of the local stress state through macroscopic variables. Phil Trans R Soc Lond A 361: 921–946

Lipton R (2004a) Homogenization and design of functionally graded composites for stiffness and strength. In: Ponte Castaneda P, Telega JJ (eds) Nonlinear homogenization and its application to composites, polycrystals, and smart materials. NATO Science series II Mathematics, Physics, and Chemestry, vol 170 Springer, Berlin Heidelberg New York, pp 169–192

Lipton R (2004b) Stress constrained G closure and relaxation of structural design problems. Q Appl Math 62:295–321

Lipton R (2004c) Homogenization theory and the assessment of extreme field values in composites with random microstructure. SIAM J Appl Math 65:475–493

Lipton R, Stuebner M (2006a) Optimization of composite structures subject to local stress constraints. Comput Methods Appl Mech Eng 196:66–75

Lipton R, Stuebner M (2006b) Inverse homogenization and design of microstructure for pointwise stress control. Q J Mech Appl Math 59:131–161

Lipton R, Velo AP (2002) Optimal design of gradient fields with applications to electrostatics. Nonlinear partial differential equations and their applications. College de France Seminar, vol 14 (Paris, 1997/1998). Stud Math Appl vol 31. North Holland, Amsterdam, pp 509–532

Love A (1944) A treatise on the mathematical theory of elasticity. Dover, New York

Lurie K (1993) Applied optimal control theory of distributed systems. Plenum Press, New York

Olhoff N (1996) On optimum design of structures and materials. Meccanica 31:143–161

Pedregal P (2004) Constrained quasiconvexification of the square of the gradient of the state in optimal design. Quart Appl Math 62:459–470

Stuebner M (2006) An inverse homogenization design method for stress control in composites. Ph.D. thesis, Louisiana State University

Tartar L (1994) Remarks on optimal design problems. In: Buttazzo G, Bouchitte G, Suquet P (eds) Calculus of variations, homogenization and continuum mechanics. World Scientific, Singapore, pp 279–296

Tartar L (2000) An introduction to the homogenization method in optimal design. Springer Lecture Notes in Mathematics, vol 1740. Springer, Berlin Heidelberg New York, pp 45–156

Velo AP (2000) Optimal design of gradient fields and currents. Ph.D. thesis, WPI